Observation of resilient propagation and free-space skyrmions in toroidal electromagnetic pulses

Ren Wang[1,2*], Pan-Yi Bao[1], Zhi-Qiang Hu[1], Shuai Shi[1], Bing-Zhong Wang[1], Nikolay I. Zheludev[3,4,5] and Yijie Shen[3,4*]

[1] *Institute of Applied Physics, University of Electronic Science and Technology of China, Chengdu 611731, China*

[2] *Yangtze Delta Region Institute (Huzhou), University of Electronic Science and Technology of China, Huzhou 313098, China*

[3] *Centre for Disruptive Photonic Technologies, School of Physical and Mathematical Sciences & The Photonics Institute, Nanyang Technological University, Singapore 637371, Singapore*

[4] *School of Electrical and Electronic Engineering, Nanyang Technological University, Singapore 639798, Singapore*

[5] *Optoelectronics Research Centre, University of Southampton, Southampton SO17 1BJ, UK*

* E-mail: rwang@uestc.edu.cn (R.W); yijie.shen@ntu.edu.sg (Y.S.)

Abstract

Toroidal electromagnetic pulses have been recently reported as nontransverse, space-time nonseparable topological excitations of free space. However, their propagation dynamics and topological configurations have not been comprehensively experimentally characterized. Also, the existing generators were limited in optical and terahertz domains, the feasibility and significance of generating such pulses at microwave frequencies have been overlooked. Here, we report that microwave toroidal pulses can be launched by a transient finite-aperture broadband horn antenna emitter. We experimentally map their topological skyrmionic textures in free space and demonstrate their resilient propagation dynamics, i.e., how that during propagation the pulses evolves towards stronger space-time nonseparability and closer proximity to the canonical Hellwarth-Nouchi toroidal pulses. Our work offers practical opportunity for using topologically robust toroidal pulses as information carriers in high-capacity telecom, cell phone technology, remote sensing, and global positioning, especially where microwave frequencies are predominant.

Introduction

Topologically structured complex electromagnetic waves have been proposed as potential information and energy carriers [1-5] for ultra-capacity communications [6,7], super-resolution metrology or microscopy [8,9] and nontrivial light-matter interactions [10,11]. Toroidal structures were recently observed in scalar spatiotemporal light waves [12], and vector electromagnetic fields termed toroidal light pulses or "flying doughnuts" [13]. Toroidal electromagnetic pulses, the propagating counterparts of localized toroidal dipole excitations in matter [14], have many exciting properties such as multiple singularities [15], space-time nonseparability [16,17] and skyrmion topologies [18,19]. Moreover, toroidal light pulses can be engaged in complex interactions with matter [20,21] and couple to electromagnetic anapoles [22]. Such toroidal optical pulses were observed by converting a short radially polarized pulse on a dispersive metasurface [13]. Because achieving higher conversion efficiencies using metasurfaces is difficult for THz, Jana et al. proposed a remarkable THz toroidal pulses generation method by quantum interference control of femtosecond pulses on a nonlinear surface [23]. The toroidal pulse research works open exiting opportunities for information and energy transfer, spectroscopy and remote sensing. However, the propagation dynamics of toroidal electromagnetic pulses and detailed characterization of their topological structures have not been experimentally investigated yet, which are crucial for potential applications of toroidal pulses. In addition, the feasibility and significance of extending toroidal pulses from optical and THz domains to microwave frequencies are to be explored.

Generation of toroidal pulses in the microwave frequency range is significant due to their intriguing potential applications in cell phone technology, telecommunications, and global positioning, where microwave frequencies are predominant. The prior optical metasurface methodology to generate toroidal pulses [13] is challenging to be extended to microwave domain because of the required electrically larger aperture and collimating laser source. The quantum interference control for THz toroidal pulse emission [23] is also challenging to be applied for generating microwave toroidal pulses due to the lack of such third-order nonlinear materials in microwave frequency range. Therefore, the generation of microwave toroidal pulses remains a challenge.

In this paper, we present an effective approach to the generation of free-space microwave electromagnetic toroidal pulses with a purposely designed transient finite-aperture horn antenna emitter, like an "air cannon". Using this new technique, we experimentally study propagation dynamics of electromagnetic toroidal pulses. We observed previously unreported propagation dynamics of electromagnetic toroidal pulses that evolve towards higher proximity to the canonical Hellwarth-Nouchi toroidal electromagnetic pulse during propagation. We conducted vectorial spatiotemporal mapping of the electric field of the pulse and demonstrate that their topological configurations are robust over a long distance. The high quality of the generated electromagnetic toroidal pulses allowed experimental observation of free-space electromagnetic skyrmions embedded in the Hellwarth-Nouchi canonical solution.

Results

Generation scheme for microwave toroidal pulses. The toroidal pulses that we will call canonical Hellwarth-Nouchi pulses are space-time nonseparable, non-transverse propagating electromagnetic excitation, the exact solution of Maxwell's equations in the form first found by Hellwarth and Nouchi in 1996 [24]:

$$E_r = 4if_0\sqrt{\frac{\mu_0}{\varepsilon_0}}\frac{r(q_2 - q_1 - 2iz)}{[r^2 + (q_1 + i\tau)(q_2 - i\sigma)]^3}, \quad (1)$$

$$E_z = -4f_0\sqrt{\frac{\mu_0}{\varepsilon_0}}\frac{r^2 - (q_1 + i\tau)(q_2 - i\sigma)}{[r^2 + (q_1 + i\tau)(q_2 - i\sigma)]^3}, \quad (2)$$

$$H_\theta = -4if_0\frac{r(q_1 + q_2 - 2ict)}{[r^2 + (q_1 + i\tau)(q_2 - i\sigma)]^3}. \quad (3)$$

where (r, z) represents spatial cylindrical coordinate, t is time, $\sigma = z + ct$, $\tau = z - ct$, f_0 is a normalization constant, q_1 and q_2 represent the central wavelength of the wave package and the Rayleigh range, respectively. The magnetic field is azimuthal, H_θ, and the electric field include both radial and longitudinal components, E_r and E_z, forming a nontransverse wave.

Our generation scheme for microwave toroidal pulses is schematically shown in Fig. 1. The generator is a radially polarized purposely designed broadband conical coaxial horn antenna with operating frequency range of 1.3-10 GHz, see details in Supplementary Materials. It is inheritably more broadband and more accurately reproduces the canonical spectrum of Hellwarth-Nouchi pulses than the toroidal source based on segmented radial polarizer and discrete metamaterial dispersion corrector [13]. Below we will show results for generating toroidal pulses with $q_1 = 0.01$m and $q_2 = 50q_1$.

To launch toroidal electromagnetic pulse, the antenna was stimulated by an integral waveform as presented on Fig 1(b). As the antenna is a capacitive load to the feed, its output waveform is a differential of the driving signal that matches temporal profile of the desired free-space toroidal pulse with $q_2 = 0.5$ m and single cycle at $z = 0$ m.

Experiments were performed in a microwave anechoic chamber. To map the magnitude and phase distributions of the E_r components of the broadband conical coaxial horn antenna, as shown in Fig. 1(c), we used linearly polarized horn probe with operating frequency range of 1-18 GHz. The E_z component was retrieved using Gauss's law, see the details in Supplementary Materials.

Observation of propagation dynamics of toroidal pulses. Fig. 2 shows the spatiotemporal evolutions of experimentally measured, numerically simulated and canonical Hellwarth-Nouchi toroidal electromagnetic pulses at propagation distances of 5 cm, 50 cm, and 100 cm, respectively, from the horn aperture.

The conical coaxial horn antenna generates in free space an electromagnetic field of rotational symmetry around the propagation direction. From Fig. 2, it is evident that both the measured waveforms and the waveforms simulated by time-domain Maxwell solving follow a pattern similar to that of canonical Hellwarth-Nouchi pulses, transitioning from a single cycle to 1½ cycles [25]. As the bandwidth of our antenna is limited, the durations of experimentally observed pulses are somewhat larger than the canonical Hellwarth-Nouchi pulses with the same values of q_1 and q_2.

The spectral distributions at positions 5 cm, 50 cm, and 100 cm along a specific radius are depicted in Fig. 3. The spectral composition in simulated, experimental measurements, and canonical Hellwarth-Nouchi pulses spread outward with propagation and the locations of spectral maxima at different frequencies are gradually moving apart, revealing the isodiffraction characteristic [16,17].

The toroidal electromagnetic pulse's isodiffraction characteristic, relevant to space-time nonseparability [16], is evaluated to assess how it evolves after radiating from the antenna, as shown in Fig. 4. The measured state-tomography matrix $\{c_{i,j}\}$, with element $c_{i,j} = \int \varepsilon_{\eta_i}\varepsilon^*_{\lambda_j} dr$ representing the overlap of spatial and spectral states, indicates a poor match to the canonical Hellwarth-Nouchi pulse at proximity to the antenna and it gradually diagonalizes upon propagation, where ε_{λ_j} and ε_{η_i} describe the distributions of monochromatic energy density and total energy density [16]. The concurrence $con = \sqrt{2[1 - Tr(\rho_A^2)]}/\sqrt{2(1 - 1/n)}$ and entanglement of formation $EoF = -Tr[\rho_A \log_2(\rho_A)]/\log_2(n)$, where n and ρ_A are respectively state dimension and the reduced density matrix [26], corresponding to the simulated and measured toroidal electromagnetic pulses quickly increase and remain above 0.9 with distance. Both simulated and measured fidelity $F = Tr(M_1 M_2)$ [27], where M_1 and M_2 are respectively the density matrices for the generated and canonical Hellwarth-Nouchi toroidal pulse, at z = 0.65 m exceeds 0.7 (see supplementary materials for details), indicating a high spatiotemporal nonseparability, akin to Hellwarth-Nouchi pulses with noise [16]. Therefore, during propagation the experimentally generated pulses evolves towards stronger space-time nonseparability and closer proximity to the canonical Hellwarth-Nouchi pulse.

The propagation dynamics of toroidal pulses is related to their isodiffraction characteristic [16]. Indeed, various frequency components of toroidal pulses spatially diffract at a same rate upon propagation, i.e. the relative radial positions of frequencies components remain invariance during propagation. In contrast, in non-isodiffraction broadband signals some frequencies may leave the beam during propagation. This explains why imperfect electromagnetic toroidal pulses generated by the antenna evolve towards the canonical Hellwarth-Nouchi solution: the non-isodiffractive frequency components of the pulse scatter away while the isodifractive canonical components persists. Such robustness makes toroidal pulses promising information carrier candidates.

Observation of skyrmionic textures imbedded in toroidal pulses. The dynamics of localized electromagnetic skyrmions has been reported on structured plasmonic interfaces [28-29]. Moreover, it was recently understood that skyrmionic textures are also imbedded in toroidal electromagnetic pulses [18]. However, such structures have never been observed experimentally before. Here we provide experimental mapping of these fields. Fig. 5 displays maps of the experimental vector fields, with highlighting of the measured skyrmionic textures at distances of 5 cm, 50 cm, and 100 cm from the antenna aperture. As expected, the electric field has both radial component E_r and longitudinal component E_z. The field features vector singularities, including saddle points on central axis ("longitudinal-toward radial-outward" or "radial-toward longitudinal-outward", marked by "△") and vortex rings away from the central axis (surrounding electric vector forming a vortex loop, marked by "○"). The skyrmionic textures are varying but with preserved Néel-type helicity at different transverse planes. The skyrmionic textures can be observed at the planes located at the front or the back (not too far away) of the electromagnetic vortex ring's center. Additionally, the skyrmionic number's sign "±" alternates on either side of the saddle points. For example, Néel-type skyrmionic textures exist in the transverse planes marked by green dashed lines, where the electric vector changes its direction from "down/up" at the center to "up/down" away from the center. Indeed, the skyrmion number of measured and simulated toroidal is always approximately ±1, as appropriate for skyrmionic textures. The coverage of the sphere of field vectors for measured, simulated, and canonical Hellwarth-Nouchi toroidal pulses fully spans the surface of the sphere, providing a confirmation of the presence of skyrmions, the calculation method of which we used is similar to that of the recent observation of continue-sound-wave skyrmions [30], see details in Supplementary Materials.

Discussion

In conclusion, we presented a simple and efficient scheme for generating microwave toroidal pulse using a radially-polarized conical horn antenna like an electromagnetic cannon. We investigated propagation of toroidal pulses and mapped their skyrmionic structure. We demonstrated that during free-space propagation the pulses evolve towards higher space-time nonseparability and closer proximity to the canonical Hellwarth-Nouchi toroidal pulses. In addition to the coaxial cone-shaped horn emitter, we investigated coaxial pentagonal, coaxial rectangular, and coaxial triangular horns, as illustrated in supplementary materials. Despite the different shapes of these coaxial horns, all emitted similar space-time field and spectrum distributions resembling the canonical Hellwarth-Nouchi toroidal pulse. The coaxial configuration inherently provides radial polarization and wide bandwidth emission, which are critical factors for generating toroidal pulses. The scheme can also generate azimuthally polarized microwave toroidal pulses by substituting the inner and outer conductors with artificial magnetic conductors.

We argue that horn antennas offer practical opportunity for using robust toroidal pulses as information carriers in high-capacity telecom applications and remote sensing. The free-space toroidal pulses are of interest to information transfer as much as localized skyrmions are of interest to data storage in topological matter [31-34]. The skyrmion textures within toroidal pulses are space-time skyrmions in free space, distinct from other skyrmion textures found in free space, structured media, and evanescent waves [19]. The single-cycle waveform, skyrmionic quasi-particle topology and their propagation resilience are crucial for ensuring robustness against environmental disturbances in high-capacity telecommunications. For realizing such information transfer lines coaxial horn antenna may be used as receiver of toroidal pulses, although their efficiency and the ability to discriminate between toroidal pulses and conventional transverse pulses will have to be investigated. In addition, the propagation dynamics indicates that the unique spectrum signature at each position within the toroidal field and the unique polarization signature within the skyrmionic texture can be utilized as tags for determining the coordinates of targets in detection applications.

Moreover, the propagation dynamics, particularly the progression towards canonical Hellwarth-Nouchi toroidal pulses, offer multiple avenues for the generation of toroidal pulses. Contrasted with the field distribution of canonical Hellwarth-Nouchi toroidal pulses at the z=0 position, the field distribution at the aperture of the broadband conical coaxial horn antenna manifests two distinct characteristics: a smaller aperture and a singular signal excitation. Under these circumstances, its radiative field can still gradually transform into toroidal pulses during propagation. Furthermore, in the supplementary materials, we explore the propagation dynamics of toroidal pulses under aperture truncation, uniform distribution, and random distribution cases. Under all these cases, the space-time nonseparability of electromagnetic toroidal pulses evolves towards higher levels and closer resemblance to the canonical form during propagation, even when the remaining energy after truncation is merely 1.9% of the original electromagnetic toroidal pulses. This reveals that the resilient propagation of toroidal pulses does not depend on the coaxial horn antenna and exists regardless of whether the frequency range is microwave or optical, suggesting that strict adherence to the equations governing toroidal pulses' radiation or scattering aperture field distribution is unnecessary when designing schemes for generating supertoroidal pulses [18], nondiffracting toroidal pulses [35], helical pulses [36], and other topologically complex toroidal fields with more intricate spectra. For example, using dispersive metasurfaces, quantum interference control, or antennas, we can achieve a spectrum distribution similar to that of supertoroidal pulses. Frequencies that deviate from the canonical supertoroidal pulse may dissipate during propagation, as revealed in this paper. Therefore, imperfectly generated supertoroidal pulses have the potential to evolve towards the canonical supertoroidal solution over time.

Methods

Coaxial horn antenna design and simulation. The coaxial horn antenna is designed with CST microwave studio. The antenna comprises inner and outer conductors made of metal, with 3D-printed conical and flat-shaped dielectric supports at the bottom and top of the coaxial horn, respectively. The dielectric material possesses a dielectric constant of 1.3. To reduce the weight of the entire coaxial horn, the interior of the inner conductor is hollowed out. The antenna is fed from the bottom of the conical structure using a 2.92 mm coaxial connector with the rotationally symmetric TEM mode (radial polarization), where the inner and outer conductors of the connector are connected to the inner and outer conductors of the coaxial horn. The simulated time-domain results were obtained by directly exciting the coaxial horn antenna with the signal $g_{\mathrm{f}}(t)=\int_{-\infty}^{t}E_{\mathrm{r}}(\tau,r=r_{\mathrm{f}},\mathrm{z}=0)\,d\tau$ based on the canonical Hellwarth-Nouchi toroidal pulse' E_{r} component at the radius $r=r_{\mathrm{f}}$ with the widest spectral range on the z=0 m plane.

Measurement method. We utilized a planar microwave anechoic chamber for measuring the spatial electromagnetic fields of the broadband conical coaxial horn antenna. The antenna was moved to the desired measurement area using a scanning frame. The vector network analyzer was connected to the transmitting and receiving antennas, and we measured S_{21} to obtain the magnitude and phase characteristics of the electromagnetic field at different spatial positions. The receiving antenna used in the experiment was the broadband conical coaxial horn antenna we designed, while the transmitting antenna was a standard rectangular horn antenna with a frequency range of 1-18 GHz. Due to the rotational symmetry of the broadband conical coaxial horn antenna's structure, we only needed to measure the electric field within a rectangular region on one side along the central axis of the horn antenna. Rotating this rectangular region around the central axis by 360° provided the electric field distribution in three-dimensional space. The polarization direction of the transmitting standard horn antenna was adjusted to align with the radial direction of the broadband conical coaxial horn antenna. The scanning system was programmatically controlled to scan within the desired plane, allowing us to obtain the field distribution in the target plane.

Observation method of skyrmion textures. We used the above method to measure the E_{r} component in frequency domain, different from the methods used [13] and [23]. Due to the strict rotational symmetry of the designed broadband conical coaxial horn antenna, the electromagnetic pulses it generates consist solely of E_{r} and E_{z} components. The E_{z} component can be determined from the measured E_{r} component using a transformation formula based on Gauss's law, the same as [13]. The experimental time-domain results were acquired through spectral measurements. We obtained the spatial magnitude and phase characteristics of the broadband conical coaxial horn antenna using the aforementioned frequency domain measurement method and computed the time-domain field through inverse Fourier transformation. The combination of E_z and E_r components in the spatiotemporal field distribution enables the construction of a spatiotemporal vector field distribution, allowing for the observation of skyrmionic textures.

Supplementary Material

The supplementary material encompasses the design of the coaxial horn antenna, along with measurement techniques and outcomes pertaining to various electrical components. Additionally, it details the approach for computing time-domain fields and the methodology for assessing spatiotemporal nonseparability. The discussion in supplementary material further explores the space-time nonseparability of aperture truncated toroidal electromagnetic pulses, the spatiotemporal vector field distribution, and the implications of the coaxial horn's geometric configuration.

References

1. Nye, J. F. & Berry, M. V. Dislocations in wave trains. In A Half-Century of Physical Asymptotics and Other Di-versions: Selected Works by Michael Berry, 6–31 (World Scientific, 1974).
2. Berry, M. Making waves in physics. *Nature* **403**, 21–21 (2000).
3. He, C., Shen, Y., & Forbes, A. Towards higher-dimensional structured light. *Light: Sci. & Appl.* **11**(1) 205. (2022).

4. Bliokh, K. Y., Karimi, E., et al. Roadmap on structured waves. *J. Opt.* **25**(10), 103001 (2023).

5. Shen, Y., Zhan. Q., et al. Roadmap on spatiotemporal light fields. *J. Opt.* **25**(9), 093001 (2023).

6. Wan, Z., Wang, H., Liu, Q., Fu, X., & Shen, Y. Ultra-Degree-of-Freedom Structured Light for Ultracapacity Information Carriers. *ACS Photonics* **10**(7), 2149–2164 (2023).

7. Willner, A. E., Pang, K., Song, H., Zou, K., & Zhou, H. Orbital angular momentum of light for communications. *Appl. Phys. Rev.* **8**(4), 041312 (2021).

8. Yuan, G. H., & Zheludev, N. I. Detecting nanometric displacements with optical ruler metrology. *Science* **364**(6442), 771-775 (2019).

9. Zheludev, N. I., & Yuan, G. Optical superoscillation technologies beyond the diffraction limit. *Nat. Rev. Phys.* **4**(1), 16-32 (2022).

10. Ozawa, T. et al. Topological photonics. *Reviews of Modern Physics* **91**, 015006 (2019).

11. Price, H., Chong, Y., et al. Roadmap on topological photonics. *Journal of Physics: Photonics* **4**(3), 032501 (2022).

12. Wan, C., Cao, Q., Chen, J., Chong, A., & Zhan, Q. Toroidal vortices of light. *Nat. Photon.* **16**(7), 519-522 (2022).

13. Zdagkas, A., McDonnell, C., Deng, J., et al. Observation of toroidal pulses of light. *Nat. Photon.* **16**, 523–528 (2022).

14. Kaelberer, T., Fedotov, V. A., Papasimakis, N., Tsai, D. P., & Zheludev, N. I.. Toroidal dipolar response in a metamaterial. *Science* **330**(6010), 1510-1512 (2010).

15. Zdagkas, A., Papasimakis, N., Savinov, V., Dennis, M. R., & Zheludev, N. I. Singularities in the flying electromagnetic doughnuts. *Nanophotonics* **8**(8), 1379-1385 (2019).

16. Shen, Y., Zdagkas, A., Papasimakis, N., & Zheludev, N. I. Measures of space-time nonseparability of electromagnetic pulses. *Phys. Rev. Res.* **3**(1), 013236 (2021).

17. Shen, Y. & Rosales-Guzmán, C. Nonseparable states of light: from quantum to classical. *Laser & Photonics Reviews* **16**(7), 2100533 (2022).

18. Shen, Y., Hou, Y., Papasimakis, N., & Zheludev, N. I. Supertoroidal light pulses as electromagnetic skyrmions propagating in free space. *Nat. Commun.* **12**(1), 5891 (2021).

19. Shen, Y., Zhang, Q., Shi, P., Du, L., Zayats, A. V., & Yuan, X. Optical skyrmions and other topological quasiparticles of light. *Nat. Photon.* **18**, 15–25 (2024).

20. Raybould, T., Fedotov, V. A., Papasimakis, N., Youngs, I., & Zheludev, N. I. Exciting dynamic anapoles with electromagnetic doughnut pulses. *Appl. Phys. Lett.* **111**(8), 081104 (2017).

21. Papasimakis, N., Fedotov, V. A., Savinov, V., Raybould, T. A., & Zheludev, N. I. Electromagnetic toroidal excitations in matter and free space. *Nat. Mater.* **15**(3), 263-271(2016).

22. Fedotov, V. A., Rogacheva, A. V., Savinov, V., Tsai, D. P., & Zheludev, N. I.. Resonant transparency and non-trivial non-radiating excitations in toroidal metamaterials. *Sci. Rep.* **3**(1), 2967 (2013).

23. Jana, K., Mi, Y., Møller, S. H., et al. Quantum control of flying doughnut terahertz pulses. *Sci. Adv.* **10**(2), eadl1803 (2024).

24. Hellwarth, R. W. & Nouchi, P. Focused one-cycle electromagnetic pulses. *Phys. Rev. E* **54**, 889–895 (1996).

25. Raybould, T., Fedotov, V., Papasimakis, N., Youngs, I., & Zheludev, N. Focused electromagnetic doughnut pulses and their interaction with interfaces and nanostructures. *Opt. Express* **24**(4), 3150-3161 (2016).

26. Rungta, P., Bužek, V., Caves, C. M., Hillery, M., & Milburn, G. J., Universal state inversion and concurrence in arbitrary dimensions, *Phys. Rev. A* **64**, 042315 (2001).

27. James, D. F. V., Kwiat, P. G., Munro, W. J., & White, A. G., On the measurement of qubits, in Asymptotic Theory of Quantum Statistical Inference: Selected Papers (World Scientific, Singapore, 2005), pp. 509–538.

28. Tsesses, S., Ostrovsky, E., Cohen, K., Gjonaj, B., Lindner, N. H., & Bartal, G. Optical skyrmion lattice in evanescent electromagnetic fields. *Science*, **361**(6406), 993-996(2018).

29. Davis, T. J., Janoschka, D., Dreher, P., Frank, B., Meyer zu Heringdorf, F. J., & Giessen, H. Ultrafast vector imaging of plasmonic skyrmion dynamics with deep subwavelength resolution. *Science*, **368**(6489), eaba6415(2020).

30. Muelas-Hurtado, R. D., Volke-Sepúlveda, K., Ealo, J. L., et al. Observation of polarization singularities and topological textures in sound waves. *Phys. Rev. Lett.* **129**, 204301 (2022).

31. Fert, A., Reyren, N., & Cros, V. (2017). Magnetic skyrmions: advances in physics and potential applications. *Nat. Rev. Mater.* **2**, 17031 (2017).

32. Bogdanov, A. N. & Panagopoulos, C. Physical foundations and basic properties of magnetic skyrmions. *Nat. Rev. Phys.* **2**, 492-498 (2020).

33. Bernevig, B. A., Felser, C., & Beidenkopf, H. Progress and prospects in magnetic topological materials. *Nature*, **603**(7899), 41-51 (2022).

34. Han, L., Addiego, C., et al. High-density switchable skyrmion-like polar nanodomains integrated on silicon. *Nature*, **603**(7899), 63-67 (2022).

35. Shen, Y., Papasimakis, N., & Zheludev, N. I.. Nondiffracting supertoroidal pulses: optical "Kármán vortex streets". *Nat. Commun.* **15**, *4863* (2024).

36. Lekner, J.. Helical light pulses. *Journal of Optics A: Pure and Applied Optics*, **6**(10), L29 (2004).

Acknowledgments

This work has been supported by the National Natural Science Foundation of China (62171081, 61901086), the Natural Science Foundation of Sichuan Province (2022NSFSC0039), European Research Council (FLEET-786851), Singapore Ministry of Education (MOE) AcRF Tier 1 grant (RG157/23, RT11/23). Y. S. also acknowledges the support from Nanyang Technological University Start Up Grant.

Author contributions

R.W. conceived the ideas and supervised the project, R.W., P.Y.B. and Z.Q.H. performed the theoretical modeling and numerical simulations, R.W. developed the experimental methods, P.Y.B., Z.Q.H. and R.W. conducted the experimental measurements, R.W., P.Y.B., S.S. and Y.S. conducted data analysis. All authors wrote the manuscript and participated the discussions.

Competing interests

The authors declare no competing financial interests.

Data and materials availability

The data that support the findings of this study are available from the corresponding author upon reasonable request.

Additional information

Supplementary information is available for this paper. Correspondence and requests for materials should be addressed to R.W. and Y.S..

Figures

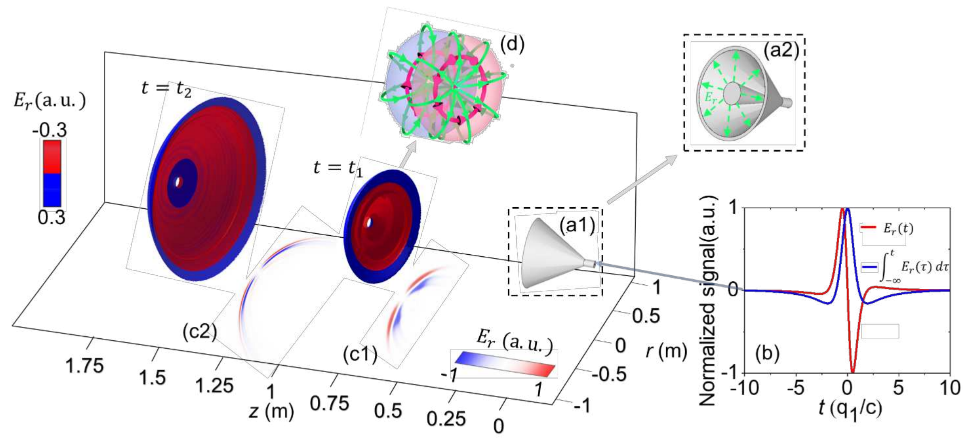

Fig. 1. Generation of toroidal pulses from a "microwave cannon". (a) Cylindrical coaxial antenna horn, front (a1) and back views (a2). (b) Driving voltage applied to the antenna feed (blue line) and transient antenna output (red line). (c) The simulated spatiotemporal evolution of the toroidal pulse: (c1) and (c2) are the spatial isosurfaces of the electric field at two different moments of time; (d) schematic of the electromagnetic configuration of the toroidal pulse.

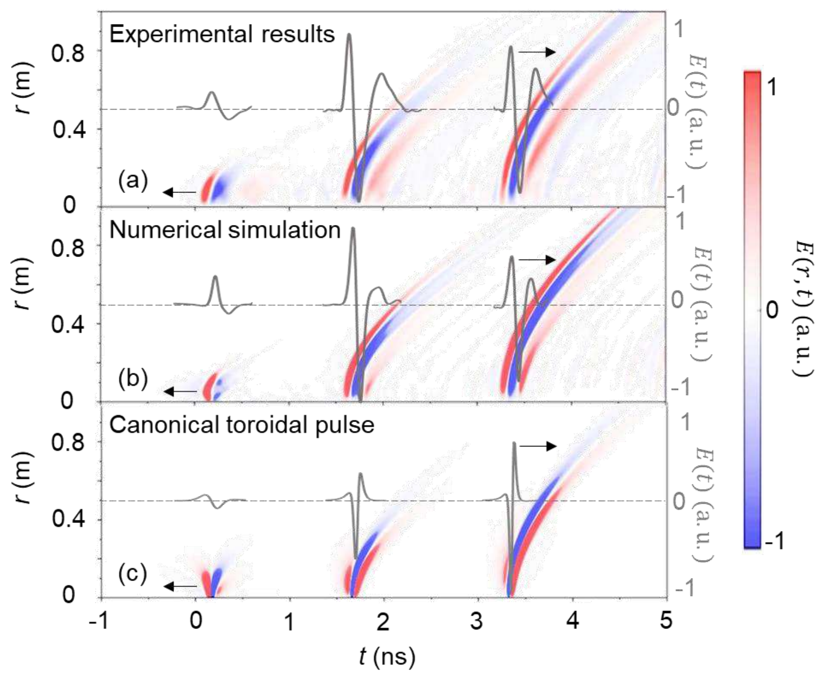

Fig. 2. Spatiotemporal evolution of toroidal pulses. (a) Experimental and (b) numerically simulated spatiotemporal evolution of the amplitude E_r of the pulses launched by the antenna compared to (c) canonical Hellwarth-Nouchi toroidal pulses. The gray curves indicate the electric field at approximately $r = 0.2$ m.

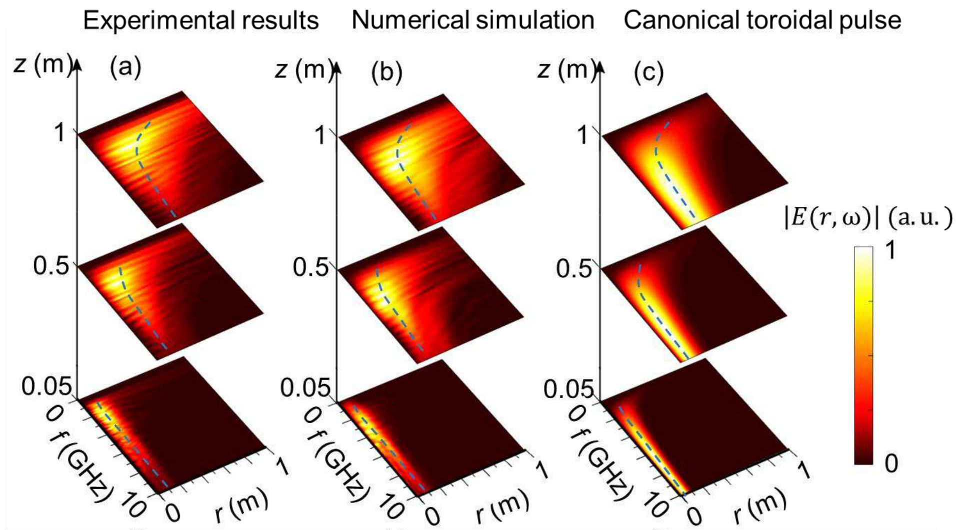

Fig. 3. Spectral distributions of E_r field at variant propagation distances. (a) Experimental data, (b) numerical simulation, and (c) canonical Hellwarth-Nouchi pulses. The blue dashed lines track the spectrum maximum.

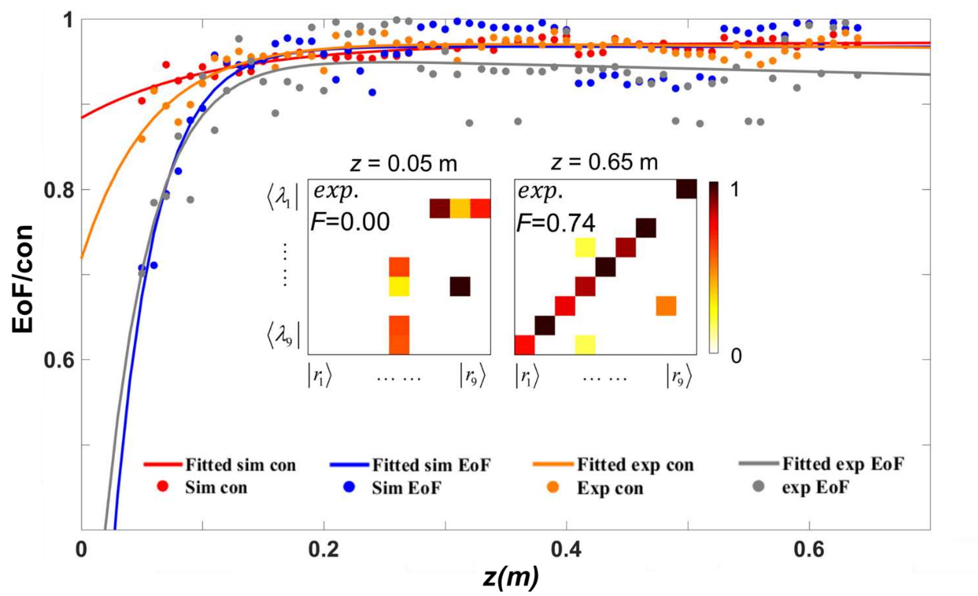

Fig. 4. Space-time nonseparability. The dots and fitting curves indicate numerically simulated and experimentally measured values of concurrence (con) and entanglement of formation (EoF) of the generated toroidal pulses versus propagation distance. The con and EoF quickly increase and remain above 0.9 with distance, and the inserted experimental state-tomography matrix shows a poor match to the canonical Hellwarth-Nouchi pulse at z = 0.05 m and it diagonalizes at z = 0.65 m, indicating the generated pulses evolves towards stronger space-time nonseparability and closer proximity to the canonical Hellwarth-Nouchi pulse during propagation.

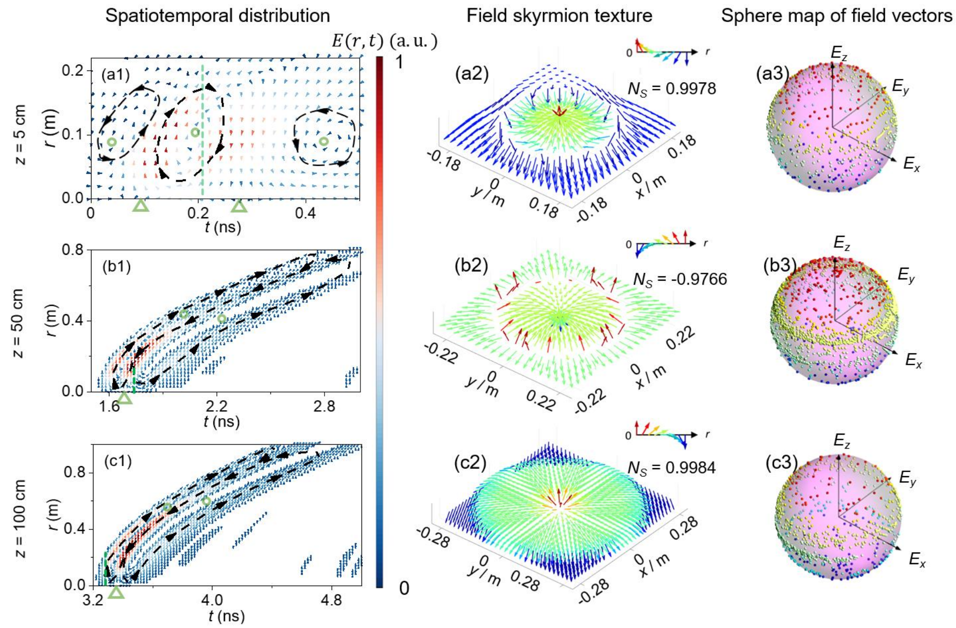

Fig. 5. Experimental spatiotemporal distribution of vector fields. Green tringles and circles in (b1) and (c1) mark the positions of saddle points and vortex rings, respectively. The green dashed lines in (a1), (b1) and (c1) respectively indicate the positions of the skyrmionic textures in (a2), (b2) and (c2) at specific times on the *xy* plane. In (a2), (b2) and (c2), the skyrmion number (*NS*) is approximately 1, which signifies well-defined skyrmionic textures. The skyrmionic textures are varying but with preserved Néel-type helicity at different transverse planes. The coverage of the sphere of field vectors in (a3), (b3) and (c3), respectively corresponding to the skyrmionic textures in (a2), (b2) and (c2), spans the surface of the sphere, providing a confirmation of the presence of skyrmions.